7/31/20

Mechanisms associated with Daytime and Nighttime Heat Waves over the Contiguous United States

Natalie P. Thomas*[1,2], Michael G. Bosilovich[2], Allison B. Marquardt Collow [1,2], Randal D. Koster [2], Siegfried D. Schubert[2,3], Amin Dezfuli [2,3], Sarith P. Mahanama [2,3]

[1]Universities Space Research Association, Columbia, MD
[2]Global Modeling and Assimilation Office, NASA Goddard Space Flight Center, Greenbelt MD
[3]Science Systems and Applications, Inc., Lanham, MD

Revised submission to Journal of Applied Meteorology and Climatology on 31 July 2020

* *Corresponding address*: Global Modeling and Assimilation Office, Code 610.1 NASA Goddard Space Flight Center, Greenbelt, MD 20771, natalie.p.thomas@nasa.gov

ABSTRACT

Heat waves are extreme climate events that have the potential to cause immense stress on human health, agriculture, and energy systems, so understanding the processes leading to their onset is crucial. There is no single accepted definition for heat waves, but they are generally described as a sustained amount of time where temperature exceeds a local threshold. Multiple different temperature variables are potentially relevant, as high values of both daily maximum (Tmax) and minimum (Tmin) temperatures can be detrimental to human health. In this study, we focus explicitly on the different mechanisms associated with summertime heat waves manifested during daytime versus nighttime hours over the contiguous United States. Heat waves are examined using the National Aeronautics and Space Administration (NASA) Modern-Era Retrospective analysis for Research and Applications, Version 2 (MERRA-2). Over 1980–2018, the increase in the number of heat wave days per summer was generally stronger for nighttime heat wave days than daytime heat wave days, with localized regions of significant positive trends. Processes linked with daytime and nighttime heat waves are identified through composite analysis of precipitation, soil moisture, clouds, humidity and fluxes of heat and moisture. Daytime heat waves are associated with dry conditions, reduced cloud cover, and increased sensible heating. Mechanisms leading to nighttime heat waves differ regionally across the US, but they are typically associated with increased clouds, humidity and/or low-level temperature advection. In the Midwest US, enhanced moisture is transported from the Gulf of Mexico during nighttime heat waves.

1. Introduction

Heat waves are among the most destructive extreme climate events, causing immense stress on human health, agriculture, and energy systems. The study of heat waves is complicated by the lack of a single accepted definition for them (Robinson 2001; Perkins and Alexander 2012; Perkins 2015). They are broadly defined as a sustained amount of time where temperature exceeds a threshold. However, a variety of different temperature variables can be used – the daily mean (Tmean), maximum (Tmax) and minimum (Tmin) temperature are potentially relevant, as are variables which account for humidity (Russo et al. 2017), such as apparent temperature, equivalent temperature, and heat index. Smith et al. (2013) and Lyon and Barnston (2017) provide detailed comparisons of these different indices.

Previous research has indicated that, on a global scale, heat wave frequency and intensity have increased (Perkins et al. 2012) and are likely to continue to increase in the future (Meehl and Tebaldi 2004; Wang et al. 2020). Over the United States, trends in heat wave frequency have been generally positive in recent decades (Oswald and Rood 2014; Schoof et al. 2017; Oswald 2018; Shafiei Shiva et al. 2019), although regional trends vary based on the index used (Smith et al. 2013). Several studies have noted the greater increase in nighttime (Tmin) versus daytime (Tmax) heat waves over the United States (Lyon and Barnston 2017; Rennie et al. 2019), specifically over California and Nevada (Gershunov et al. 2009), the Pacific Northwest (Bumbaco et al. 2013) and Florida (Cloutier-Bisbee et al. 2019).

The health impacts of extreme daytime heat are intuitive, but epidemiological studies have also noted the particularly dangerous nature of nighttime heat. In several case studies over different regions, minimum temperatures were more strongly linked with excess mortality (Kalkstein and Davis 1989; Kalkstein 1991; Hajat et al. 2002; Dousset et al. 2011). Presumably, this is due to the fact that warm nights eliminate the anticipated recovery period during extreme heat events. Both daytime and nighttime heat waves can be harmful to society, so it is important to understand the unique mechanisms leading to the onset of each.

Atmospheric conditions characteristic of daytime heat waves are well-studied. Typically, heat waves are associated with anticyclonic circulation and subsidence in the middle and upper troposphere (Namias 1982; Chang and Wallace 1987; Meehl and Tebaldi 2004; Lau and Nath 2012; Schubert et al. 2014; Grotjahn et al. 2016; Yang et al. 2019). Horizontal temperature advection is also an important driver, and the relative contributions of subsidence and advection can vary even between geographically close regions (e.g., Hu et al. 2019; Yang et al. 2019). Several studies have shown the potential for Rossby wave patterns to influence extreme events such as heat waves in different parts of the world (Schubert et al. 2011; Wu et al. 2012; Teng et al. 2013; Kornhuber et al. 2019; Röthlisberger et al. 2019). Lehmann and Coumou (2015) reported a link between storm track activity and heat extremes. For daytime heat waves, land-atmosphere interactions are also highly relevant, as daytime heat leads to depletion of soil moisture and a subsequent reduction in evaporative cooling (Fischer et al. 2007; Miralles et al. 2014). Thus, droughts and heat waves are often linked, although the strength of the linkage varies regionally (Koster et al. 2009; Cheng et al. 2019).

Relatively fewer studies have focused on the mechanisms associated with nighttime heat waves. Nighttime heat waves have typically been linked with an anomalously moist atmosphere, which affects downward longwave fluxes. Gershunov et al. (2009) found a similar atmospheric circulation during daytime and nighttime heat waves over California but greater moisture advection from offshore during the latter. In their study of heat waves over the Pacific Northwest US, Bumbaco et al. (2013) also noted a greater role of precipitable water in nighttime heat waves, compared with a stronger 500-hPa ridge and increased subsidence during daytime heat waves. Over the Korean peninsula, nighttime heat events were found to be associated with a baroclinic atmospheric structure and increased cloud cover (Hong et al. 2018). A comprehensive analysis of mechanisms driving nighttime heat waves for different regions of the United States does not yet exist, to the best of our knowledge.

In this study, we focus explicitly on the different mechanisms associated with heat waves manifested during daytime versus nighttime hours over the United States. To facilitate this separation, the majority of the analysis will concentrate on events that occur solely during either the daytime or nighttime hours. Events that span both daytime and nighttime hours muddle the interpretation of independent processes, and hence are not the primary focus here. Section 2 describes the data and analysis methods. Section 3 details the results, starting with an assessment of the climatology and trends in heat wave frequency over the United States, and followed by a composite analysis to investigate mechanisms that contribute to heat waves. A summary and conclusions are provided in section 4.

2. Data and methods

a. MERRA-2

The National Aeronautics and Space Administration (NASA) Modern-Era Retrospective analysis for Research and Applications, Version 2 (MERRA-2; Gelaro et al. 2017) is the primary tool used in this analysis. Hourly data from MERRA-2 are available at a spatial resolution of 0.625° longitude by 0.5° latitude starting in January 1980.

MERRA-2 is a global atmospheric reanalysis with a variety of updates relative to the original MERRA (Rienecker et al. 2011). Among these is the inclusion of an observation-driven precipitation field to force the land surface (Reichle et al. 2017a). An evaluation of the MERRA-2 climate can be found in Bosilovich et al. (2015). In general, MERRA-2 is improved relative to its predecessor, though biases do remain. For instance, MERRA-2 often underestimates the daily maximum temperature and overestimates the daily minimum temperature, leading to a negative bias in the diurnal temperature range (Bosilovich et al. 2015; Draper et al. 2018). MERRA-2 typically reproduces notable summer precipitation anomalies over the US, though issues exist with the diurnal cycle of precipitation[1] (Bosilovich et al. 2015). Although in general the inclusion of observation-corrected precipitation improves the estimates of land surface hydrology and energy balance (Reichle et al. 2017b; Draper et al. 2018), the downwelling longwave (net shortwave) radiation at the surface tends to be underestimated (overestimated) over the US (Bosilovich et al. 2015; Draper et al. 2018) and positive biases exist in the summer latent heat flux, particularly over energy-limited climate regimes (Draper et al. 2018).

Despite these biases, MERRA-2 provides a quality reanalysis and a useful tool for this study. The availability of a variety of diagnostics at hourly frequency allows for a better representation of diurnal variations, and makes possible a precise day/night delineation, as is necessary for this analysis.

[1] The diurnal cycle of the observation-corrected precipitation is model-generated as only daily mean values of observed precipitation contribute to the correction.

b. Heat wave definition

Rather than using Tmax and Tmin as has been done in previous studies to define heat waves, we use average daytime and average nighttime temperature to emphasize the sustained nature of heat wave events (Kalkstein and Davis 1989). Furthermore, using daytime- and nighttime-averaged temperature eliminates inconsistencies in the hour of Tmax and Tmin from day to day in a given location (Wang and Zeng 2013). Daytime and nighttime temperatures are computed using incoming shortwave flux at the top of the atmosphere (TOA) as a mask. A day begins at local sunrise, which is assumed to be the first hour in which TOA shortwave flux exceeds 10 W m^{-2}; the day ends 23 hours later. Temperatures during hours for which the TOA shortwave flux exceeds 10 W m^{-2} are averaged to produce a single daytime value, and those during hours for which TOA shortwave flux is less than 10 W m^{-2} are averaged to produce the nighttime value.

A heat wave event is defined here as a period of at least 3 days where the average 2-meter temperature (T2m) exceeds its calendar day 90^{th} percentile. There were no major changes in the results when varying the heat wave definition from 2 to 4 days. While other percentiles could be used to define heat waves, the 90^{th} percentile was chosen to provide a balance between representing extreme temperatures and maintaining a large enough sample size of events. Calendar day percentiles are computed using a fixed climatological period (1981–2010) and a five-day window (i.e., Zhang et al. 2005). We define three independent categories of heat wave events:

1. Daytime heat wave event: daytime temperature exceeds its 90^{th} percentile value for at least 3 days; nighttime temperature is below the 90^{th} percentile value on at least one of the three days.

2. Nighttime heat wave event: nighttime temperature exceeds its 90th percentile value for at least 3 days; daytime temperature is below the 90th percentile value on at least one of the three days.
3. Compound heat wave event: both daytime and nighttime temperatures exceed their 90th percentiles for at least three days.

This heat wave categorization is similar to several recent studies of heat waves over China (Freychet et al. 2017; Chen and Li 2017; Chen and Zhai 2017; Su and Dong 2019), except that here we are using daytime and nighttime average temperature rather than Tmax and Tmin. See Fig. A1 for a schematic illustrating each heat wave type. We also tested the effect of increasing the separation between daytime and nighttime temperatures in the heat wave definition, i.e., requiring that the daytime temperature is below the Xth percentile on nighttime heat wave days, and vice versa. Increasing the separation (decreasing X further below 90) reduced the number of heat wave days without changing the results notably, so X was kept at 90 in the interest of maximizing the sample size.

Heat waves are defined both on a gridpoint scale and a regional scale. For the gridpoint analysis, daytime or nighttime T2m at an individual gridpoint is used to define heat waves. For the regional analysis, daytime or nighttime T2m is area-averaged over the region of interest, and this time series is used to define heat waves over the region. The use of area-averaged temperatures for defining heat waves could lead to the situation where regional events are disproportionately influenced by extreme temperatures in only one part of the region. To address this, we examined including an additional fraction of area requirement, but found that this reduced the sample size without qualitatively changing results. We examine the continental US

(CONUS) regions used in the fourth National Climate Assessment (NCA; Wuebbles et al. 2017). See Figure A2 for further details on the process used to define heat wave days and events.

c. Analysis method

This analysis focuses on the North American warm season of June, July and August (JJA) for 1980–2018. To analyze different variables which may be linked with daytime or nighttime heat waves, we utilize composite analysis. For this, daily averages of variables are averaged over all heat wave days of a particular type, to determine dominant patterns of association. To be included in the composite analysis for independent daytime (nighttime) heat waves, a day must 1) be part of a daytime (nighttime) heat wave event (see section 2b) and 2) have only the daytime (nighttime) temperature exceed the 90th percentile (i.e., filled-in squares in Figure A2).

Composites are produced by averaging the variable of choice over all heat wave days of a given type. Thus, for a given variable, there are six composite fields: daytime-average of daytime heat wave days, nighttime average following daytime heat wave days, daytime average preceding nighttime heat wave days, nighttime average of nighttime heat wave days, daytime average of compound heat wave days and nighttime average of compound heat wave days.

Statistical significance of composites is assessed in two ways. First, a Student's t-test is performed with a null hypothesis that the composite mean anomaly is not significantly different from zero. The t-statistic is computed as the ratio of the mean of all values included in the composite to the standard error of all values included in the composite. Next, the nonparametric two-sided Wilcoxon-Mann-Whitney rank-sum test is used to assess whether heat wave days are significantly different from all summer days for a given variable. Both significance tests are performed at the 95% confidence level.

To create daily averages of variables, hourly variables are separated into their daily daytime and nighttime averages. This is done at each grid point, in the same way as for T2m described in section 2b. For analysis of NCA regions, the start of the day was taken as the most frequently occurring sunrise hour in the region on a given day. Daily daytime and nighttime anomalies are computed (using their respective climatologies) for the relevant variable using a 5-day window and a fixed climate period of 1981–2010. In the case of T2m, standardized anomalies are computed by dividing the anomalies by their standard deviation, in order to account for the local variability of temperature.

Examined variables include low level winds, 500hPa heights, vertically integrated moisture transport, precipitation, root-zone soil moisture, sensible and latent heat flux, total precipitable water, 2m specific humidity, downwelling longwave flux, cloud cover and shortwave and longwave cloud radiative effect (CRE).

Shortwave CRE (SWCRE) is calculated as the difference between the surface net downward shortwave flux (SWGNT, using MERRA-2 output variable names) and the surface net downward shortwave flux assuming clear sky (SWGNTCLR):

$$\mathrm{SWCRE} = \mathrm{SWGNT} - \mathrm{SWGNTCLR}. \quad (1)$$

Longwave CRE (LWCRE) is calculated as the difference between the surface absorbed longwave radiation (LWGAB) and the model-defined surface absorbed longwave radiation assuming clear sky, i.e. with cloud effects removed (LWGABCLR):

$$\mathrm{LWCRE} = \mathrm{LWGAB} - \mathrm{LWGABCLR}. \quad (2)$$

3. Results

a. Heat wave climatology and trends in MERRA-2

Prior to the examination of heat wave climatology, we assess the climatology of summer daytime and nighttime T2m. Figure 1 shows the mean and subseasonal standard deviation of daily daytime and nighttime T2m over all JJA days in 1980–2018. The subseasonal standard deviation is computed after removing the annual cycle and detrending the daily T2m values. The mean T2m generally decreases with latitude, with the exception of the high-elevation areas in the Rocky and Appalachian mountain ranges. The spatial patterns of daytime and nighttime mean T2m are similar, although the diurnal temperature range (difference between Figs. 1a and 1b) is larger in the western half of the country. The standard deviation of daily temperature is largest in the Northern Great Plains and Northwestern US for both daytime and nighttime T2m (Figs. 1 c,d).

The boundaries of the seven NCA regions are drawn in each panel of Fig. 1. For each of these regions, Fig. 2 displays the number of daytime, nighttime and compound heat wave days and events, as well as the average and maximum event duration for JJA 1980–2018. In all regions, there are many more compound heat wave days and events than either independent daytime or nighttime ones (Figs. 2a,b). Compound heat wave events also typically persist for longer than either daytime or nighttime events (Fig. 2c). The statistics for the Southern Great Plains are affected by the extreme summer of 2011, when 82 days in JJA were classified as heat wave days, including one single event which lasted 44 days (Fig. 2d). Therefore, the grey bars in Fig. 2 show the statistics for compound heat waves over the Southern Great Plains if 2011 is not included. The Northwest, Northern Great Plains and Southeast have the fewest number of independent day or night heat waves.

Figure 3 shows the total number of daytime, nighttime and compound heat wave days and events over JJA 1980–2018 at each grid point. Again, the most striking aspect is the high number of compound heat wave days and events (relative to daytime or nighttime days and events) at all grid points. Broadly speaking, the regions with greater variability in summertime daily T2m (Figs. 1c,d) have fewer daytime or nighttime heat wave days. In many regions, there are more daytime than nighttime heat wave days and events, especially in the Northeast, Midwest and Southwest. The Southern Great Plains stand out as having the greatest number of compound heat wave days, again with a sizeable contribution from the summer of 2011. The minimum in heat wave frequency over the North-Central US has also been noted by Lyon and Barnston (2017), who attribute it to the large day-to-day variability in atmospheric circulation in this region.

The linear trend in the number of heat wave days per summer (JJA) over 1980–2018 is shown in Fig. 4. For daytime-only heat wave days, trends are weak, varied and mostly insignificant across the U.S. (Fig. 4a). For nighttime heat wave days, trends are predominantly increasing in the Southwestern and Northwestern U.S., the Midwest and the Northeast, though statistical significance is localized and scattered within these regions and may be difficult to separate from statistical noise (Fig. 4b). The stronger and more widespread trends in nighttime versus daytime heat waves are consistent with recent literature (Oswald et al. 2018; Rennie et al. 2019). Over much of the United States, trends in the frequency of compound heat wave days (Fig. 4c) are much larger than trends in daytime or nighttime heat wave days, with a coherent region of statistically significant trends in the Western US. The northern Great Plains and parts of the Southeastern US show negative trends in compound heat wave frequency, though they are not statistically significant. This is reminiscent of the warming hole over the Southeastern US during the second half of the twentieth century (Meehl et al. 2012). Over parts of the Southwest, Northwest, Southern Plains and Northeast, trends in the frequency of compound heat wave days exceed 2 days per decade.

b. Point-wise composites

Using heat wave days at each grid point as the sample size (see Fig. 2), we compute composite fields of various variables from MERRA-2. Figure 5 shows the composites of daytime and nighttime T2m standardized anomalies for each of the three heat wave types. Compound heat wave days exhibit the largest positive standardized anomalies in T2m of all heat wave types for both daytime temperature (Fig. 5e) and nighttime temperature (Fig. 5f). Daytime T2m standardized anomalies are typically 1.25–1.75 K over the US on daytime-only heat wave days (Fig. 5a) and exceed 2 K over parts of the north-central US on compound heat wave days (Fig. 5e). As expected, the daytime T2m standardized anomalies preceding nighttime heat waves (Fig. 5c) are the weakest of the three (since by definition these temperatures must not exceed the 90th percentile), but they are still positive everywhere, ranging from 0.5–1 K. Similarly, the nighttime T2m standardized anomalies following daytime-only heat waves (Fig. 5b) are the weakest of the three nighttime temperature composites, but these too are still positive everywhere. Nighttime T2m standardized anomalies range from 1.25–1.75K on nighttime heat wave days (Fig. 5d), and from 1.5–2 K during compound heat wave days (Fig. 5f).

It is clear that compound heat wave days are associated with larger daytime and nighttime T2m anomalies than either daytime or nighttime heat wave days. However, the processes driving high daytime and nighttime temperatures during compound heat waves are not fully understood. Likely, these compound events are associated with some combination of the mechanisms driving extreme daytime or nighttime heat, with variation from one event to the next. In order to more cleanly examine the different mechanisms associated with extreme daytime and nighttime heat, the remainder of the composite analysis will focus on independent daytime and nighttime events, with some discussion of compound events throughout.

Figure 6 shows the composites of daily precipitation and root-zone soil moisture anomalies for daytime and nighttime heat wave days. Daytime heat wave days are associated with negative anomalies in daytime precipitation (Fig. 6a) and soil moisture (Fig. 6c) over the majority of the US. This is consistent with previous work noting the importance of land-surface processes for extreme high daytime temperatures (Fischer et al. 2007; Miralles et al. 2014). For nighttime heat wave days, positive nighttime precipitation (Fig. 6b) and soil moisture (Fig. 6d) anomalies are seen in the Northeast and Midwest US. Ford and Schoof (2017) also found oppressive (high humidity) heat waves in Illinois to be associated with increased antecedent precipitation and soil moisture. The positive anomalies over the agriculture-heavy Midwest suggest a potential role for evapotranspiration from crops, though further analysis is needed to better understand this relationship. Weak but significant dry anomalies persist on nighttime heat wave days over the south-central US. Compound heat wave days (not shown) are characterized by patterns resembling those of daytime heat wave days – negative anomalies in precipitation and soil moisture over the entire US, with stronger anomalies in the eastern half of the country.

Heat flux anomalies on heat wave days are shown in Fig. 7. Since heat fluxes are smaller at night, the left two columns of the figure show heat fluxes during daytime hours for both daytime and nighttime heat wave days. On daytime heat wave days, the spatial patterns of latent heat flux (Fig. 7a) and sensible heat flux (Fig. 7b) are consistent with that for soil moisture (Fig. 6c); decreased soil moisture over much of the eastern half of the US naturally leads to decreased latent heat flux and increased sensible heat flux. The Pacific Northwest and northern New England are exceptions to this, since in these regions it is energy availability, rather than water availability, which most affects evapotranspiration (Koster et al. 2006b, their Fig. 4a). Consistent with Yang et al. (2019), anomalous energy fluxes on daytime heat waves are relatively smaller over the Western US. For the daytime hours preceding nighttime heat waves (Fig. 7, middle column), latent heat flux anomalies are varied and mostly insignificant over the northern US, while sensible heat flux anomalies are significantly negative over the Northeast, Midwest, California and the Pacific Northwest (Fig. 7e). The Southern Great Plains region exhibits unique behavior, in that both daytime and nighttime heat wave days are associated with significant negative anomalies in latent heat flux and significant positive anomalies in sensible heating. This is a region characterized by strong land-atmosphere coupling (Koster et al. 2006a); air temperature variations here are in part controlled by soil moisture variations and soil moisture here is anomalously low on both daytime and nighttime heat wave days (Fig. 6d).

The right column of Fig. 7 shows the heat flux anomalies at night during nighttime heat wave days. The magnitudes of heat fluxes are much smaller at night (note the different colorbars). As Fig. 7f shows, during nighttime heat wave days over much of the central US there are significant negative anomalies in sensible heat flux at night, i.e., increased flux of heat from the air to the surface. This is reflective of the increased wind speed over these regions on nighttime heat wave days, a feature that also appears during the nighttime of compound heat wave days (not shown).

Cloud properties are examined in Fig. 8. Figure 8a shows the composites of anomalies in total cloud area fraction and demonstrates that daytime heat wave days are associated with reduced daytime cloud cover over the entire US. Nighttime heat wave days are associated with positive anomalies in total cloud area over the Northeast, Midwest and Southwest both during concurrent nighttime hours (Fig. 8b) and preceding daytime hours (Fig. 8c). Cloud cover anomalies are insignificant over the Southeast and Central US on nighttime heat wave days. The middle and bottom rows of Fig. 8 show the anomalies in shortwave and longwave cloud radiative effect (CRE).

The increased cloud cover during the daytime hours preceding nighttime heat wave days is reflected in negative anomalies in Shortwave CRE over California, the Northeast and the Midwest (Fig. 8e), or reduced shortwave radiation reaching the surface. The longwave CRE anomalies are only significantly positive over the Southwest US, with no corresponding signature in the Northeast and Midwest (Figs. 8g,h). This can be explained by Fig. 9, which shows nighttime heat wave days over the Midwest and Northeast are associated with significant increases in TPW (Fig. 9b) and near-surface specific humidity (Fig. 9d). The downwelling longwave flux at the surface is enhanced over the entire US on nighttime heat wave days, with particularly strong positive anomalies in the Southwest, Northeast and Midwest (Fig. 9f). Over the Northeast and Midwest, the increase in downwelling longwave flux is primarily associated with the increased atmospheric moisture, whereas over the Southwest, the increase in cloud fraction also plays a role. The strong positive anomalies in TPW on nighttime heat wave days (Fig. 9b) are consistent with previous studies that have noted statistically significant positive anomalies in TPW over Southern California (Gershunov et al. 2009) and the Pacific Northwest (Bumbaco et al. 2013) on Tmin-heat wave days.

c. Regional composites

The gridpoint-by-gridpoint compositing method used in Figs. 6–9 is useful for assessing patterns across the entire US and for determining regions with similar local and columnar properties. To examine large scale features of the atmospheric circulation that may contribute to regional heat waves, we look into heat waves defined using area-averaged temperatures from each of the NCA regions. Although circulation could be composited using heat waves defined at an individual grid cell, spatial averaging is likely to provide greater statistical significance to any remote connections. To represent the synoptic circulation and low-level temperature advection, respectively, Fig. 10 shows the 500-hPa heights and height anomalies and 10m wind anomaly fields composited over heat wave days for each of the seven NCA regions. In order to focus on dynamical processes rather than the influence of long-term changes, the trends are removed from 500-hPa heights prior to computation of these composites. In all regions, both daytime and nighttime heat wave days are associated with positive anomalies in 500-hPa heights, as expected (Namias 1982; Chang and Wallace 1987; Loikith and Broccoli 2012). However, there are features of the 10m winds that differ between daytime and nighttime heat waves for various regions.

The wind anomalies are relatively small during both daytime and nighttime heat waves in the Northwest and Southwest regions. Warm air advection (in particular, anomalous southerly flow) appears to be a factor in nighttime heat wave days over the Northeast, Southeast, Midwest and Southern and Northern Great Plains. (Figs. 10b,d,f,h,j). To confirm this, Fig. 11 shows the composite mean 2m temperature and 10m winds. Indeed, this displays that particularly for the Midwest (Fig. 11h) and Great Plains (Fig. 11 k,n), warmer temperatures are transported into the region by low-level southern winds on nighttime heat wave days.

The strong wind anomalies during nighttime heat wave days over the Midwest US (Fig. 10f) are interesting given that this region consistently showed noteworthy anomalies in other variables on nighttime heat wave days in the gridpoint composites: increased precipitation and soil moisture (Figs. 6b,d), reduced sensible heating (Fig. 7d), increased cloud cover (Figs. 8b,c), and increased humidity and TPW (Figs. 9b,d). The Great Plains Low Level Jet (GPLLJ; Bonner 1968) is an important player in the summer hydroclimate of the US, as it transports heat and moisture from the Gulf of Mexico into the central US. It is characterized by a wind maximum in the lower troposphere and a diurnal cycle with increased strength at nighttime (Helfand and Schubert 1995; Weaver and Nigam 2008). In order to investigate reasons for increased moisture in the Midwest region on nighttime heat wave days, composites of 850-hPa winds and vertically integrated moisture transport over Midwest heat wave days are shown in Fig. 12. Given the climatological diurnal variability of these quantities, this figure shows the nighttime fields for both daytime and nighttime heat wave days to facilitate a direct comparison.

Figure 12 shows that nighttime 850-hPa winds over the Great Plains and Midwest US are much stronger for nighttime heat waves (Fig. 12b) than for daytime heat waves (Fig. 12a), suggesting a strengthened GPLLJ. For nighttime heat waves, nighttime 850-hPa winds exceed 16 m/s in the Central Great Plains. The intensified nighttime winds are not unique to the 850-hPa level; this feature persists throughout the lower troposphere, and these increased low-level winds lead to a strong enhancement in the moisture transport into the region (Fig. 12d). The nighttime heat wave wind fields are reminiscent of the first mode of GPLLJ variability identified by Weaver and Nigam (2008), corresponding to a strengthening and northward extension of the jet (see their Fig. 10), leading to positive precipitation anomalies in the Midwest and negative precipitation anomalies in the Southeast US. Previous studies have found the terminus of the GPLLJ to be connected with the development of mesoscale convective systems (Tuttle and Davis 2006), which could offer further connection to the positive anomalies in precipitation on nighttime heat wave days. The structure of the 500-hPa height anomaly pattern for Midwest nighttime heat waves (Fig. 10f) consists of a slightly eastward-displaced ridge and a trough to the west, indicating a coupling between the upper level flow and low-level jet (e.g., Burrows et al. 2019). This suggests a greater role for synoptic scale rather than boundary-layer processes in driving the strengthened GPLLJ. It has also been shown that the presence of a mid-tropospheric cyclone/anticyclone spanning the continent (as seen in Fig. 10f) amplifies the diurnal component of the GPLLJ (Schubert et al. 1998). The anomalous continental-scale ridge characteristic of daytime heat wave events (Fig. 10e) allows daytime temperatures to climb from increased solar radiation, and nighttime temperatures to radiatively cool.

4. Summary and conclusions

This study examined daytime, nighttime and compound heat waves during summer over the United States using MERRA-2. Compound heat waves occurred the most frequently over the United States during JJA 1980–2018 and are associated with the largest daytime and nighttime temperature anomalies. Despite this, independent daytime or nighttime heat wave events present an opportunity to assess unique processes driving extreme temperatures during daytime or nighttime separately, and thus are the focus of this analysis. Such an approach was further motivated by the particularly dangerous nature of high nighttime temperatures and by the larger trends in the frequency of nighttime versus daytime heat waves over many regions (Fig. 4). We constructed composites of various land surface and atmospheric variables for these two types of heat waves to infer their mechanisms.

The results for daytime heat waves are generally consistent with previous research on heat waves: they are associated with positive anomalies in 500-hPa heights, dry soils, a lack of precipitation, reduced cloud cover and increased sensible heating. Exact processes do vary between different regions of the US, with a greater role indicated for surface energy fluxes in the central and eastern US (Yang et al. 2019).

Mechanisms associated with nighttime heat waves differ by region. In the Great Plains and Southeast, nighttime heat wave days are associated with anomalous low-level southerly flow (Figs. 9d,h,j), leading to the advection of warmer air into the region. In the Northeast, Midwest and Southwest US, nighttime heat wave days are associated with increased cloud cover and TPW, which keeps daytime temperatures lower due to reduced solar radiation at the surface and leads to increased downward longwave flux at the surface at night (Fig. 9f). This is again consistent with previous explanations for extreme nighttime heat over the Pacific Northwest of the US (Bumbaco et al. 2013), China (Chen and Li 2017) and Korea (Hong et al. 2018).

The Northeast and Midwest US exhibit unique behavior on nighttime heat wave days – in addition to increased clouds and moisture, they are associated with positive anomalies in precipitation and soil moisture. Further investigation of the Midwest US revealed that increased low-level winds on nighttime heat wave days bring increased moisture from the Gulf of Mexico into the region. The apparent connection between the GPLLJ and heat waves in the Midwest US is noteworthy. The development of a GPLLJ significantly affects heat and moisture transports over the US (Uccellini and Johnson 1979; Helfand and Schubert 1995) and thus is a logical potential influence on heat waves. Lopez et al. (2018) found an enhanced GPLLJ to be linked with fewer heat extremes in the Great Plains through its influence on soil moisture. However, their study focused on heat waves defined using daily mean temperature; their results would likely have been different if they had defined heat waves using minimum temperatures.

Mechanisms driving nighttime heat wave days in the Northwest US remain unclear. It is possible that nighttime heat waves in this region are simply the result of warm daytime temperatures that haven't quite exceeded the 90th percentile, similar to the reasoning for dry tropical nights provided by Chen et al. (2014). This can be seen in Fig. 5c, which shows that daytime T2m anomalies preceding nighttime heat wave days are greatest in the Northwest and Great Plains. Additionally, there are relatively few heat wave days over the Northwest US during this period (see Fig. 3), leading to a small sample size for the composite analysis.

It should be noted that results here are for summer heat waves in general; how the mechanisms linked with heat waves vary between the summer months of June, July and August would be an interesting question, although a larger sample size would be required.

It would be worthwhile to examine other potential remote influences on daytime and nighttime heat waves using composite analysis or other methods. For instance, the frequency of heat waves over the United States has been recently linked to the Atlantic Multidecadal Variability (Ruprich-Robert et al. 2018), the North Atlantic Subtropical High (Li et al. 2019) and Arctic sea ice extent (Budikova et al. 2019). Lopez et al. (2019) found a potential linkage between circulation associated with heat waves in the U.S. Great Plains and the East Asian Monsoon through a stationary wave-train forced by diabatic heating. However, all of these studies were focused on Tmax-or Tmean-type heat waves; teleconnective influences on independent nighttime heat waves remain to be examined.

In general, the present analysis identifies unique processes associated with daytime and nighttime extreme temperatures over most regions, justifying their separate study. Compound heat waves, those events manifested in both the daytime and nighttime temperatures, had the most frequent occurrence (Figs. 2–3), greatest frequency trends (Fig. 4) and strongest intensity (Fig. 5) of the three heat wave types. These events were not given as much attention in this analysis in order to cleanly distinguish the processes associated with the daytime and nighttime extremes. It is hypothesized that individual compound events arise due to some combination of the unique daytime or nighttime heat processes identified in this study. Further work is needed to understand the temporal evolution of daytime and nighttime temperatures and the accumulation of heat during compound heat waves.

5. Acknowledgments

This work was supported by NASA Earth Science: National Climate Assessment Enabling Tools program. MERRA-2 was developed under the NASA Modeling Analysis and Prediction program. We thank three anonymous reviewers for their constructive feedback on the manuscript.

Data availability statement: MERRA-2 data can be obtained from the NASA GESDISC.

6. Appendix: Heat Wave Definition

Figure A1 provides an example of each of the three heat wave types. In the top left panel, one of the three nights (in this example, the third one) falls below the 90^{th} percentile, so this would be classified as a daytime heat wave. The top right panel is an example of a nighttime heat wave since the first two days are below the 90^{th} percentile while all three nights exceed the 90^{th} percentile. In the bottom left panel, both daytime and nighttime temperature exceed their 90^{th} percentile on all three days, satisfying the definition of a compound heat wave. The bottom right panel is not a heat wave since neither daytime nor nighttime temperature exceeds the 90^{th} percentile on all three days.

Figure A2 then illustrates how heat wave days and events are identified given a time series of daily 2mdaytime or nighttime temperature. For the gridpoint analysis, this is the daily temperature at an individual grid point. For the regional-scale analysis, this is T2m area-averaged over the NCA region of choice. The example outlined here is for heat waves in the Northeast US NCA region.

Daytime and nighttime temperatures are analyzed separately to define heat wave days. For each calendar day in JJA, days are identified where T2m exceeds its calendar-day 90th percentile for 3 days or more. If only one of daytime or nighttime temperatures is in heat wave conditions on a given day, it is an independent daytime or nighttime heat wave day (filled red and blue squares in Fig. A2). If both daytime and nighttime temperatures are in heat wave conditions, a compound heat wave day is identified (filled-in black squares in Fig. A2).

Heat wave events are identified next. If a collection of consecutive heat wave days consists only of daytime or nighttime heat wave days, it is defined as a daytime or nighttime event, as indicated by the red and blue lines in Fig. A2. If a collection of consecutive heat wave days consists of only compound heat wave days, or any combination of daytime, nighttime and compound heat wave days, it is classified as a compound heat wave event (black lines in Fig. A2).

Finally, for daytime and nighttime heat wave days, the opposite temperature is examined to ensure that it is below the 90th percentile. By definition there will not be 3 consecutive days where the opposite temperature exceeds the 90th percentile (otherwise it would be a compound heat wave). However, it is still possible that for individual days in the event, the opposite temperature exceeds the 90th percentile. These are shown by the unfilled red and blue squares in

Fig. A2. These days are excluded from the composite analysis of independent daytime and nighttime heat waves, but still remain as part of the daytime or nighttime event.

7. References

Bonner, W.D., 1968: Climatology of the Low Level Jet. *Monthly Weather Review*, **96**, 833–850.

Bosilovich, M. G., and Coauthors, 2015: MERRA-2: Initial evaluation of the climate. NASA Tech. Memo. NASA/TM-2015-104606/Vol. 43, 145 pp. [Available online athttps://gmao.gsfc.nasa.gov/pubs/docs/Bosilovich803.pdf.]

Budikova, D., T.W. Ford and T.J. Ballinger, 2019: United States Heat Wave Frequency and Arctic Ocean Marginal Sea Ice Variability. *Journal of Geophysical Research*, **124**.

Bumbaco, K.A., K.D. Dello and N.A. Bond, 2013: History of Pacific Northwest Heat Waves: Synoptic Patterns and Trends. *Journal of Applied Meteorology and Climatology*, **52**, 1618–1631.

Burrows, D.A., C.R. Ferguson and M.A. Campbell, 2019: An objective classification and analysis of upper-level coupling to the Great Plains low-level jet over the 20th century. *Journal of Climate*, **32**, 7127–7152.

Chang, F-C., and J.M. Wallace, 1987: Meteorological Conditions during Heat Waves and Droughts in the United States Great Plains, *Monthly Weather Review*, **115**, 1253–1269.

Chen, R. and R. Lu, 2014: Dry tropical nights and wet extreme heat in Beijing: Atypical Configurations between High Temperature and Humidity. *Monthly Weather Review*,**142**, 1792–1802.

Chen, Y. and Y. Li, 2017: An Inter-comparison of Three Heat Wave Types in China during 1961–2010: Observed Basic Features and Linear Trends. *Scientific Reports*, **7**, 45619.

Chen, Y. and P. Zhai, 2017: Revisiting summertime hot extremes in China during 1961–2015: Overlooked compound extremes and significant changes. *Geophysical Research Letters*, **44**, 5096–5103.

Cheng, L., M. Hoerling, Z. Liu and J. Eischeid, 2019: Physical Understanding of Human-Induced Changes in U.S. Hot Droughts Using Equilibrium Climate Simulations. *Journal of Climate*, **32**, 4431–4443.

Cloutier-Bisbee, S.R., A. Raghavendra and S.M. Milrad, 2019: Heat Waves in Florida: Climatology, Trends, and Related Precipitation Events. *Journal of Applied Meteorology and Climatology*, **58**, 447–466.

Dousset, B., F. Gourmelon, K. Laaidi, A. Zeghnoun, E. Giraudet, P. Bretin, E. Mauri and S. Vandentorren, 2011: Satellite monitoring of summer heat waves in the Paris metropolitan area. *International Journal of Climatology*, **31**, 313–323.

Draper, C.S., R.H. Reichle and R.D. Koster, 2018: Assessment of MERRA-2 Land Surface Energy Flux Estimates. *Journal of Climate*, **31**, 671–691.

Fischer, E.M., S.I. Seneviratne, P.L. Vidale, D. Lüthi and C. Schär, 2007: Soil Moisture-Atmosphere Interactions during the 2003 European Summer Heat Wave. *Journal of Climate*, **20**, 5081–5099.

Ford, T.W. and J.T. Schoof, 2017: Characterizing extreme and oppressive heat waves in Illinois. *Journal of Geophysical Research: Atmospheres*, **122**, 682–698.

Freychet, N., S. Tett, J. Wang and G. Hegerl, 2017: Summer heat waves over Eastern China: dynamical processes and trend attribution. *Environmental Research Letters*, **12**, 024015.

Gelaro, R., et al., 2017: The Modern-Era Retrospective Analysis for Research and Applications, Version 2 (MERRA-2). *Journal of Climate*, **30**, 5419–5454.

Gershunov, A., D.R. Cayan and S.F. Iacobellis, 2009: The Great 2006 Heat Wave over California and Nevada: Signal of an Increasing Trend. *Journal of Climate*, **22**, 6181–6203.

Grotjahn, R., R. Black, R. Leung, M.F. Wehner, M. Barlow, M. Bosilovich, A. Gershunov, W.J. Gutowski, J.R. Gyakum, R.W. Katz, Y-Y. Lee, Y-K. Lim and Prabhat, 2016: North American extreme temperature events and related large scale meteorological patterns: a review of statistical methods, dynamics, modeling and trends. *Climate Dynamics*, **46**, 1151–1184.

Hajat, S., R.S. Kovats, R.W. Atkinson and A. Haines, 2002: Impact of hot temperatures on death in London: a time series approach. *Journal of Epidemiology & Community Health*, **56**, 367–372.

Helfand, H.M. and S.D. Schubert, 1995: Climatology of the Simulated Great Plains Low-Level Jet and Its Contribution to the Continental Moisture Budget of the United States. *Journal of Climate*, **8**, 784–806.

Hong, J.-S., S.-W Yeh, and K.-H. Seo, 2018: Diagnosing physical mechanisms leading to pure heat waves versus pure tropical nights over the Korean Peninsula. *JGR Atmospheres*, **123**, 7149–7160.

Hu, L., J. Luo, G. Huang and M.C. Wheeler, 2019: Synoptic features responsible for Heat waves in Central-Africa, a region with strong multi-decadal trend. *Journal of Climate*, **32**, 7951–7970.

Kalkstein, L.S., 1991: A New Approach to Evaluate the Impact of Climate on Human Mortality. *Environmental Health Perspectives,* **96**, 145–150.

Kalkstein, L.S. and R.E. Davis, 1989: Weather and Human Mortality: An Evaluation of Demographic and Interregional Responses in the United States. *Annals of the Association of American Geographers*, **79**, 44–64.

Kornhuber, K., S. Osprey, D. Coumou, S. Petri, V. Petoukhov, S. Rahmstorf and L. Gray, 2019: Extreme weather events in early summer 2018 connected by a recurrent hemispheric wave-7 pattern. *Environmental Research Letters*, **14**.

Koster, R.D., and Co-authors, 2006a: GLACE: The Global Land-Atmosphere Coupling Experiment, Part I, Overview. *Journal of Hydrometeorology*, **7** (4), 590–610.

Koster, R.D., B.M. Fekete, G.J. Huffman and P.W. Stackhouse, 2006b: Revisiting a hydrological analysis framework with International Satellite Land Surface Climatology Project Initiative 2 rainfall, net radiation, and runoff fields. *Journal of Geophysical Research*, **111**, D22S05.

Koster, R.D., S.D. Schubert and M.J. Suarez, 2008: Analyzing the Concurrence of Meteorological Droughts and Warm Periods, with Implications for the Determination of Evaporative Regime. *Journal of Climate*, **22**, 3331–3341.

Lau, N-C. And M.J. Nath, 2012: A Model Study of Heat Waves over North America: Meteorological Aspects and Projections for the Twenty-First Century. *Journal of Climate*, **25**, 4761–4784.

Lehmann, J. and D. Coumou, 2015: The influence of mid-latitude storm tracks on hot, cold, dry and wet extremes. *Scientific Reports*, **5**, 17491.

Li, W., T. Zou, L. Li, Y. Deng, V.T. Sun, Q. Zhang, J.B. Layton and S. Setoguchi, 2019: Impacts of the North Atlantic subtropical high on interannual variation of summertime heat stress over the conterminous United States. *Climate Dynamics*, **53**, 3345–3359.

Loikith, P.C, and A.J. Broccoli, 2012: Characteristics of Observed Atmospheric Circulation Patterns Associated with Temperature Extremes over North America. *Journal of Climate*, **25**, 7266–7281.

Lopez, H., R. West, S. Dong, G. Goni, B. Kirtman, S.-K. Lee and R. Atlas, 2018: Early emergence of anthropogenically forced heat waves in the western United States and Great Lakes. *Nature Climate Change*, **8**, 414–420.

Lopez, H., S-K. Lee, S. Dong, G. Goni, B. Kirtman, R. Atlas and A. Kumar, 2019: East Asian Monsoon as a Modulator of U.S. Great Plains Heat Waves. *Journal of Geophysical Research: Atmospheres*, **124**, 6342–6358.

Lyon, B. and A.G. Barnston, 2017: Diverse Characteristics of U.S. Summer Heat Waves. *Journal of Climate*, **30**, 7827–7845.

Meehl, G. and C. Tebaldi, 2004: More Intense, More Frequent, and Longer Lasting Heat Waves in the 21st Century. *Science*, **305**, 994–997.

Meehl, G., J.M. Arblaster and G. Branstator, 2012: Mechanisms Contributing to the Warming Hole and the Consequent U.S. East-West Differential of Heat Extremes. *Journal of Climate*, **25,** 6394-6408.

Miralles, D.G., A.J. Teuling, C.C. van Heerwaarden and J. Vila-Guerau de Arellano, 2014: Mega-heatwave temperatures due to combined soil desiccation and atmospheric heat accumulation. *Nature Geoscience*, **7**, 345–349.

Namias, J., 1982: Anatomy of Great Plains Protracted Heat Waves (especially the 1980 U.S. summer drought). *Monthly Weather Review*, **110**, 824–838.

Oswald, E.M. and R.B. Rood, 2014: A Trend Analysis of the 1930–2010 Extreme Heat Events in the Continental United States. *Journal of Applied Meteorology and Climatology*, **53**, 565–582.

Oswald, E.M., 2018: An Analysis of the Prevalence of Heat Waves in the United States between 1948 and 2015. *Journal of Applied Meteorology and Climatology*, **57**, 1535–1549.

Perkins, S.E. and L.V. Alexander, 2012: On the Measurement of Heat Waves. *Journal of Climate*, **26**, 4500–4517.

Perkins, S.E., L.V. Alexander and J.R. Nairn, 2012: Increasing frequency, intensity and duration of observed global heatwaves and warm spells. *Geophysical Research Letters*, **39**, L20714.

Perkins, S.E., 2015: A review on the scientific understanding of heatwaves – Their measurement, driving mechanisms, and changes at the global scale. *Atmospheric Research***, 164–165**, 242–267.

Reichle, R. H., Q. Liu, R.D. Koster, C.S. Draper, S.P.P. Mahanama, and G.S. Partyka, 2017a: Land Surface Precipitation in MERRA-2. *Journal of Climate*, **30,** 1643–1664.

Reichle, R.H., C.S. Draper, Q. Liu, M. Girotto, S.P.P. Mahanama, R.D. Koster and G.J.M. De Lannoy, 2017b: Assessment of MERRA-2 Land Surface Hydrology Estimates. *Journal of Climate*, **30**, 2937–2960.

Rennie, J., J.E. Bell, K.E. Kunkel, S. Herring, H. Cullen and A.M. Abadi, 2019: Development of a Submonthly Temperature Product to Monitor Near-Real-Time Climate Conditions and Assess Long-Term Heat Events in the United States. *Journal of Applied Meteorology and Climatology*, **58**, 2653–2674.

Rienecker, M.M., et al., 2011: MERRA: NASA’s Modern-Era Retrospective Analysis for Research and Applications. *Journal of Climate*, **24**, 3624–3648.

Robinson, P.J., 2001: On the Definition of a Heat Wave. *Journal of Applied Meteorology,* **40**, 762–775.

Röthlisberger, M., L. Frossard, L.F. Bosart, D. Keyser and O. Martius, 2019: Recurrent Synoptic-Scale Rossby Wave Patterns and Their Effect on the Persistence of Cold and Hot Spells. *Journal of Climate*, **32**, 3207–3226.

Ruprich-Robert, Y., T. Delworth, R. Msadek, F. Castruccio, S. Yeager and G. Danabasoglu, 2018: Impacts of the Atlantic Multidecadal Variability on North American Summer Climate and Heat Waves. *Journal of Climate*, **31**, 3679–3700.

Russo, S., J. Sillmann and A. Sterl, 2017: Humid heat waves at different warming levels. *Scientific Reports*, 7: 7477.

Schoof, J.T., T.W. Ford and S.C. Pryor, 2017: Recent Changes in U.S. Regional Heat Wave Characteristics in Observations and Reanalyses. *Journal of Applied Meteorology and Climatology*, **56**, 2621–2636.

Schubert, S.D., H.M. Helfand, C-Y. Wu and W. Min, 1998: Subseasonal Variations in Warm-Season Moisture Transport and Precipitation over the Central and Eastern United States. *Journal of Climate*, **11**, 2530–2555.

Schubert, S., H. Wang and M. Suarez, 2011: Warm Season Subseasonal Variability and Climate Extremes in the Northern Hemisphere: The Role of Stationary Rossby Waves. *Journal of Climate*, **24,** 4773–4792.

Schubert, S.D., H. Wang, R.D. Koster and M.J. Suarez, 2014: Northern Eurasian Heat Waves and Droughts. *Journal of Climate*, **27**, 3169–3206.

Shafiei Shiva, J., D.G. Chandler and K.E. Kunkel, 2019: Localized Changes in Heat Wave Properties Across the United States. *Earth's Future*, **7**, 300–319.

Smith, T.T., B.F. Zaitchik and J.M. Gohlke, 2013: Heat waves in the United States: definitions, patterns and trends. *Climatic Change*, **118**, 811–825.

Su, Q. and B. Dong, 2019: Recent Decadal Changes in Heat Waves over China: Drivers and Mechanisms. *Journal of Climate*, **32**, 4215–4234.

Teng, H., G. Branstator, H. Wang, G.A. Meehl and W.M. Washington, 2013: Probability of US heat waves affected by a subseasonal planetary wave pattern. *Nature Geoscience*, **6**, 1056–1061.

Tuttle, J.D. and C.A. Davis, 2006: Corridors of Warm Season Precipitation in the Central United States. *Monthly Weather Review*, **134**, 2297–2317.

Uccellini, L.W. and D.R. Johnson, 1979: The Coupling of Upper and Lower Tropospheric Jet Streaks and Implications for the Development of Severe Convective Storms. *Monthly Weather Review*, **107**, 682–703.

Wang, A., and X. Zeng, 2013: Development of Global Hourly 0.5° Land Surface Air Temperature Datasets. *Journal of Climate*, **26**, 7676–7691.

Wang, J., Y. Chen, S.F.B. Tett, Z. Yan, P. Zhai, J. Feng and J. Xia, 2020: Anthropogenically-driven increases in the risks of summertime compound hot extremes. *Nature Communications*, **11**, 1-11.

Weaver, S.J. and S. Nigam, 2008: Variability of the Great Plains Low-Level Jet: Large-Scale Circulation Context and Hydroclimate Impacts. *Journal of Climate*, **21**, 1532–1551.

Wu, Z., H. Lin, J. Li, Z. Jiang and T. Ma, 2012: Heat wave frequency variability over North America: Two distinct leading modes, *Journal of Geophysical Research*, **117**, D02102.

Wuebbles, D.J., et al., 2017: Climate Science Special Report: Fourth National Climate Assessment. US Global Change Research Program, Washington DC, Vol 1.

Yang, Z., F. Dominguez and X. Zeng, 2019: Large and local-scale features associated with heat waves in the United States in reanalysis products and the NARCCAP model ensemble. *Climate Dynamics*, **52**, 1883–1901.

Zhang, X., G. Hegerl, F.W. Zwiers and J. Kenyon, 2005: Avoiding Inhomogeneity in Percentile-Based Indices of Temperature Extremes. *Journal of Climate*, **18**, 1641–1651.

8. List of Figures

Figure 1 Mean (top row) and subseasonal standard deviation (bottom row) of daytime 2mtemperature (left column) and nighttime 2mtemperature (right column) of all JJA days in 1980–2018 (i.e., 92*39=3588 days). The black lines denote the boundaries of the seven NCA regions, used for analysis of regional-scale heat waves.

Figure 2 Total number of (a) heat wave days, (b) heat wave events, (c) average event duration and (d) maximum event duration for each NCA region and for each of the 3 heat wave types: daytime (red bars), nighttime (blue bars) and compound (black bars) heat waves. The grey bars in the Southern Great Plains column indicate the statistics after omitting the extreme summer of 2011. Days and events are counted for JJA 1980–2018. The boundaries of the NCA regions are displayed in Figure 1.

Figure 3 Total number of daytime (left), nighttime (middle), and compound (right) heat wave days (top) and events (bottom) at each grid point over JJA 1980–2018.

Figure 4 Trends in number of summer (JJA) heat wave days for heat waves expressed during daytime (left) and nighttime (right) in MERRA-2. Trends are for 1980–2018. Trends significant at the 95% confidence level according to the Mann-Kendall test are indicated with white dots. Trend fields are smoothed once by a 9-point smoother before plotting.

Figure 5 Composites of daily standardized anomalies in daytime 2mtemperature (°C; left column) and nighttime 2mtemperature (°C right column) for daytime heat wave days (top row), nighttime heat wave days (middle row) and compound heat wave days (bottom row).

Figure 6 Composites of daily anomalies in observation corrected total precipitation (mm/day; top row) and root-zone soil moisture (dimensionless; bottom row) for daytime hours of daytime heat wave days (left column) and nighttime hours of nighttime heat wave days (right column). Regions where the composite mean is not statistically significant at the 95% confidence level are masked out.

Figure 7 Composites of daily anomalies in total latent heat flux (W m^{-2}; top row) and sensible heat flux from turbulence (W m^{-2}; bottom row) for daytime hours on daytime heat wave days (left column), daytime hours on nighttime heat wave days (middle column) and nighttime hours on nighttime heat wave days (right column). Regions where the composite mean is not statistically significant at the 95% confidence level are masked out.

Figure 8 Composites of daily anomalies in total cloud area fraction (dimensionless; top row), shortwave CRE (W m^{-2}; middle row) and longwave CRE (W m^{-2}; bottom row) for daytime hours on daytime heat wave days (left column), nighttime hours on nighttime heat wave days (middle column) and daytime hours on nighttime heat wave days (right column). Note that there is no shortwave CRE at night. Regions where the composite mean is not statistically significant at the 95% confidence level are masked out.

Figure 9 Composites of daily anomalies in total precipitable water vapor (kg m^{-2}; top row), 2mspecific humidity (g kg^{-1}; middle row) and surface downward longwave flux (W m^{-2}; bottom row) for daytime hours on daytime heat wave days (left column), and nighttime hours on nighttime heat wave days (right column). Regions where the composite mean is not statistically significant at the 95% confidence level are masked out.

Figure 10 Composites of daily anomalies of 500-hPa heights (m; shading) and 10mwinds (m/s; vectors) and daily mean 500-hPa height composites (m; grey contours) for daytime (left column) and nighttime (right column) heat wave days occurring in each NCA Region (rows). Fields are only plotted when the composite anomaly is statistically significant at the 95% confidence level. The region where area-averaged temperatures are used to find heat wave days for each region is outlined in green. See Figure 2 for the number of heat wave days incorporated into these composites for each region.

Figure 11 As in Fig. 10 but for the composites of daily 2m temperature (shading; °C) and 10m winds (vectors; m/s).

Figure 12 Composites of nighttime 850-hPa winds (m/s; top row) and nighttime vertically integrated moisture flux (kg m^{-1} s^{-1}; bottom row) for daytime (left column) and nighttime (right column) heat wave days occurring in NCA Region 3 (Midwest US, outlined in green).

Figure A1 Schematic illustrating examples for each of the heat wave definitions. The black line shows the 2m temperature for daytime (red dots) and nighttime (blue dots) on three hypothetical days. The red (blue) line shows the calendar-day 90^{th} percentiles for daytime (nighttime) 2m temperatures.

Figure A2 Heat wave days and events based on MERRA-2 2mtemperature data averaged over the Northeast NCA region. The filled in red, blue and black squares represent daytime, nighttime and compound heat wave days, respectively. The red, blue and black lines represent daytime, nighttime and compound heat wave events, respectively. Unfilled red (blue) squares represent daytime (nighttime) heat wave days where the nighttime (daytime) temperature also exceeds the 90th percentile. The numbers in parentheses in the legend indicate the number of days and events for each of the three heat wave types over JJA 1980-2018.

9. Figures

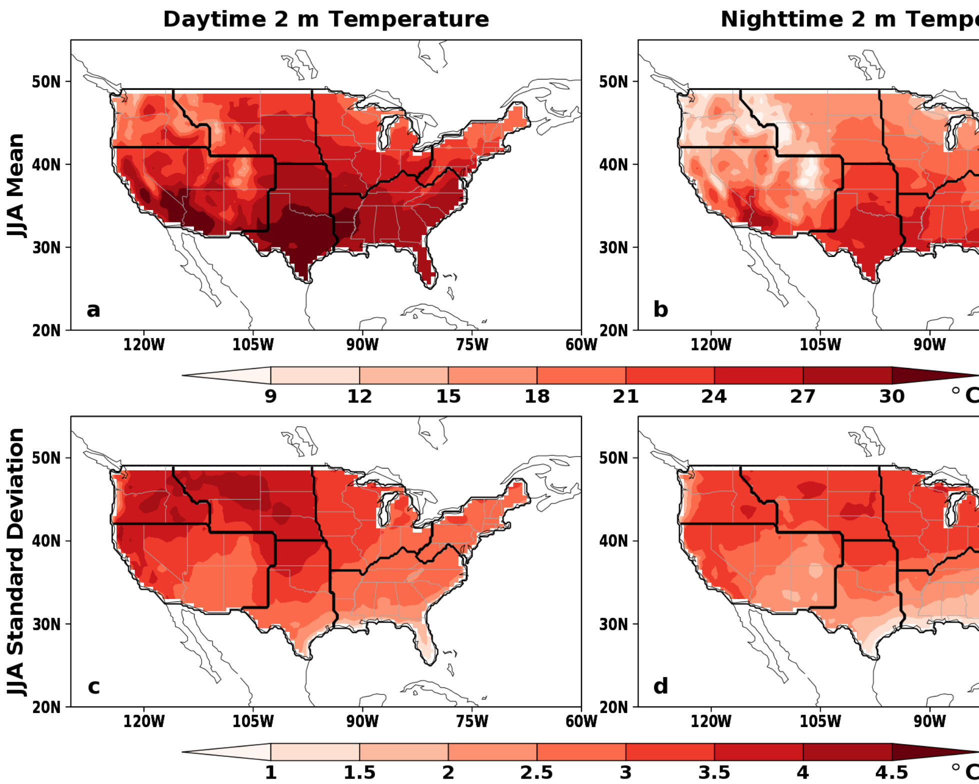

Figure 1. Mean (top row) and subseasonal standard deviation (bottom row) of daytime 2mtemperature (left column) and nighttime 2mtemperature (right column) of all JJA days in 1980–2018 (i.e., 92*39=3588 days). The black lines denote the boundaries of the seven NCA regions, used for analysis of regional-scale heat waves.

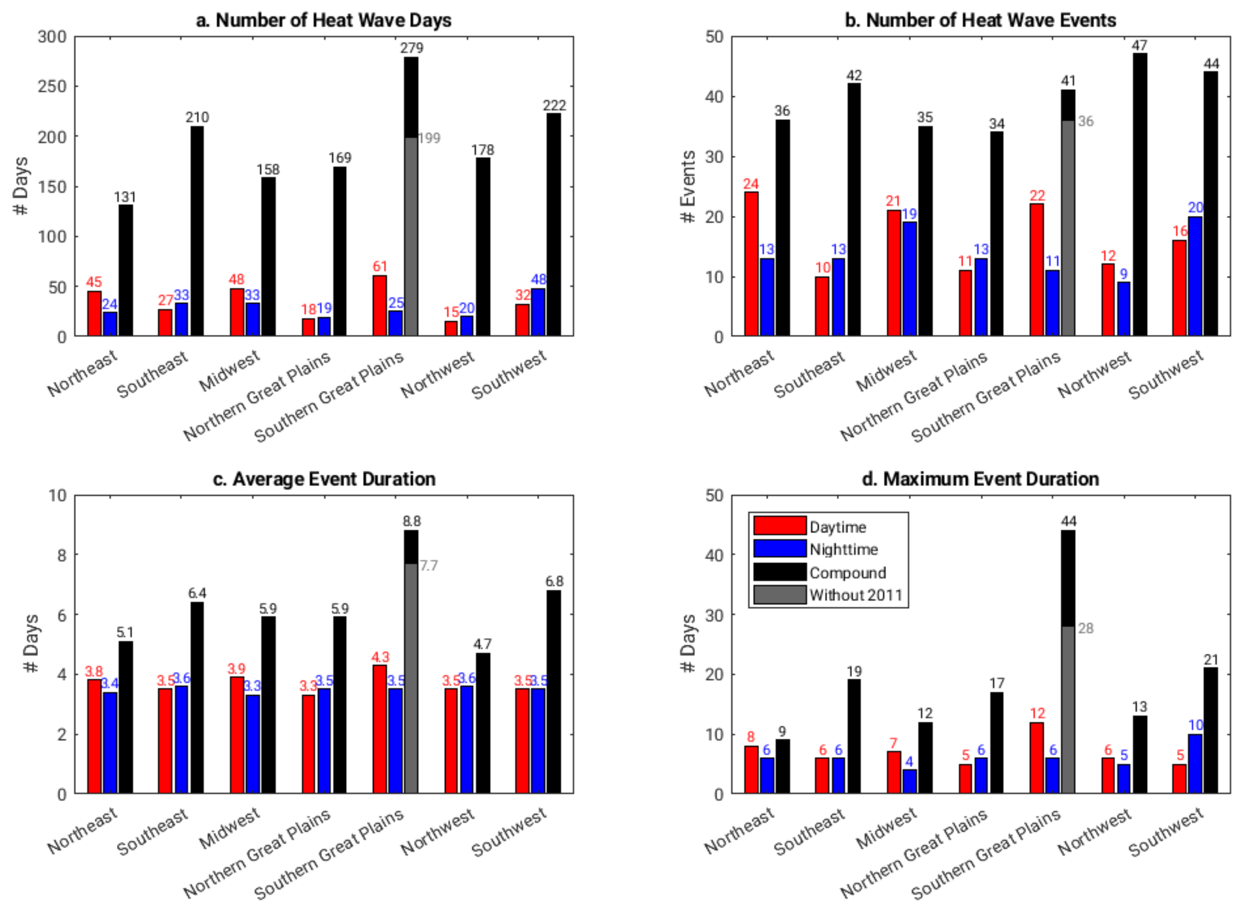

Figure 2. Total number of (a) heat wave days, (b) heat wave events, (c) average event duration and (d) maximum event duration for each NCA region and for each of the 3 heat wave types: daytime (red bars), nighttime (blue bars) and compound (black bars) heat waves. The grey bars in the Southern Great Plains column indicate the statistics after omitting the extreme summer of 2011. Days and events are counted for JJA 1980–2018. The boundaries of the NCA regions are displayed in Figure 1.

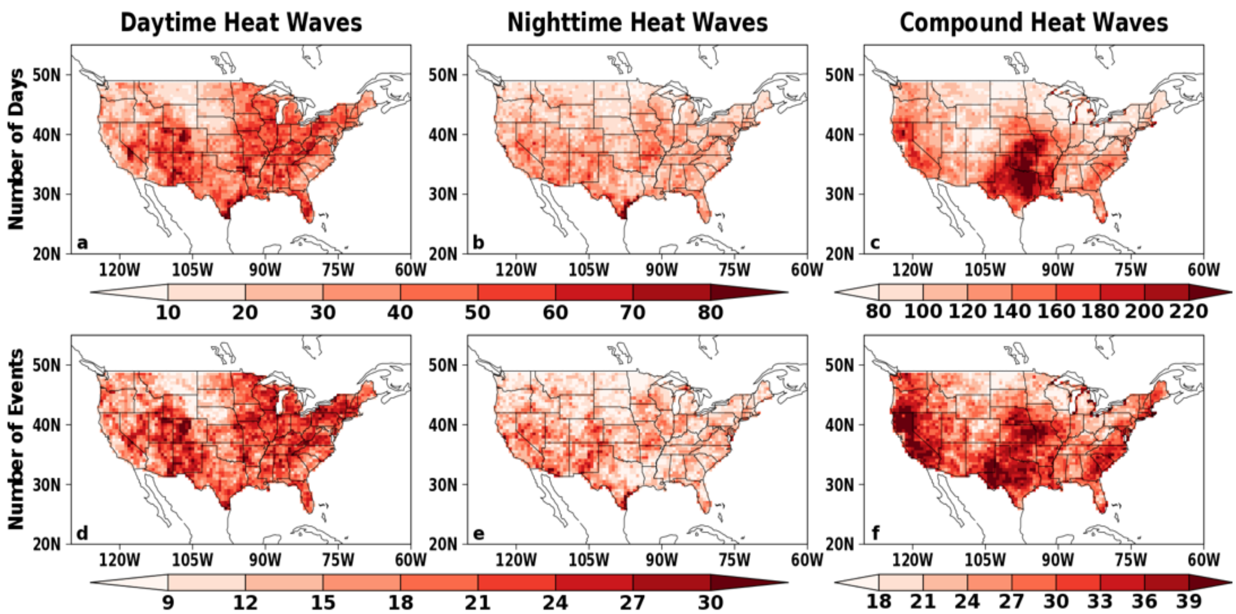

Figure 3. Total number of daytime (left), nighttime (middle), and compound (right) heat wave days (top) and events (bottom) at each grid point over JJA 1980–2018.

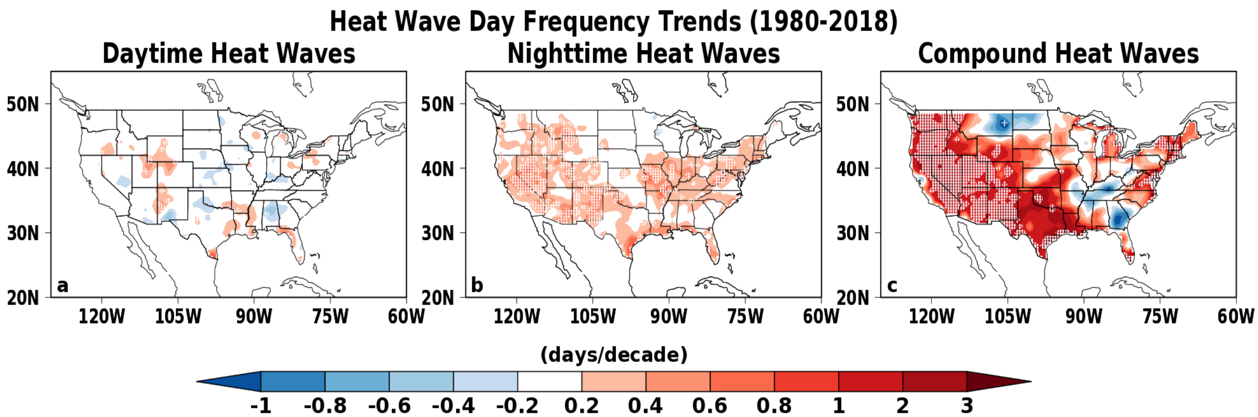

Figure 4. Trends in number of summer (JJA) heat wave days for heat waves expressed during daytime (left) and nighttime (right) in MERRA-2. Trends are for 1980–2018. Trends significant at the 95% confidence level according to the Mann-Kendall test are indicated with white dots. Trend fields are smoothed once by a 9-point smoother before plotting.

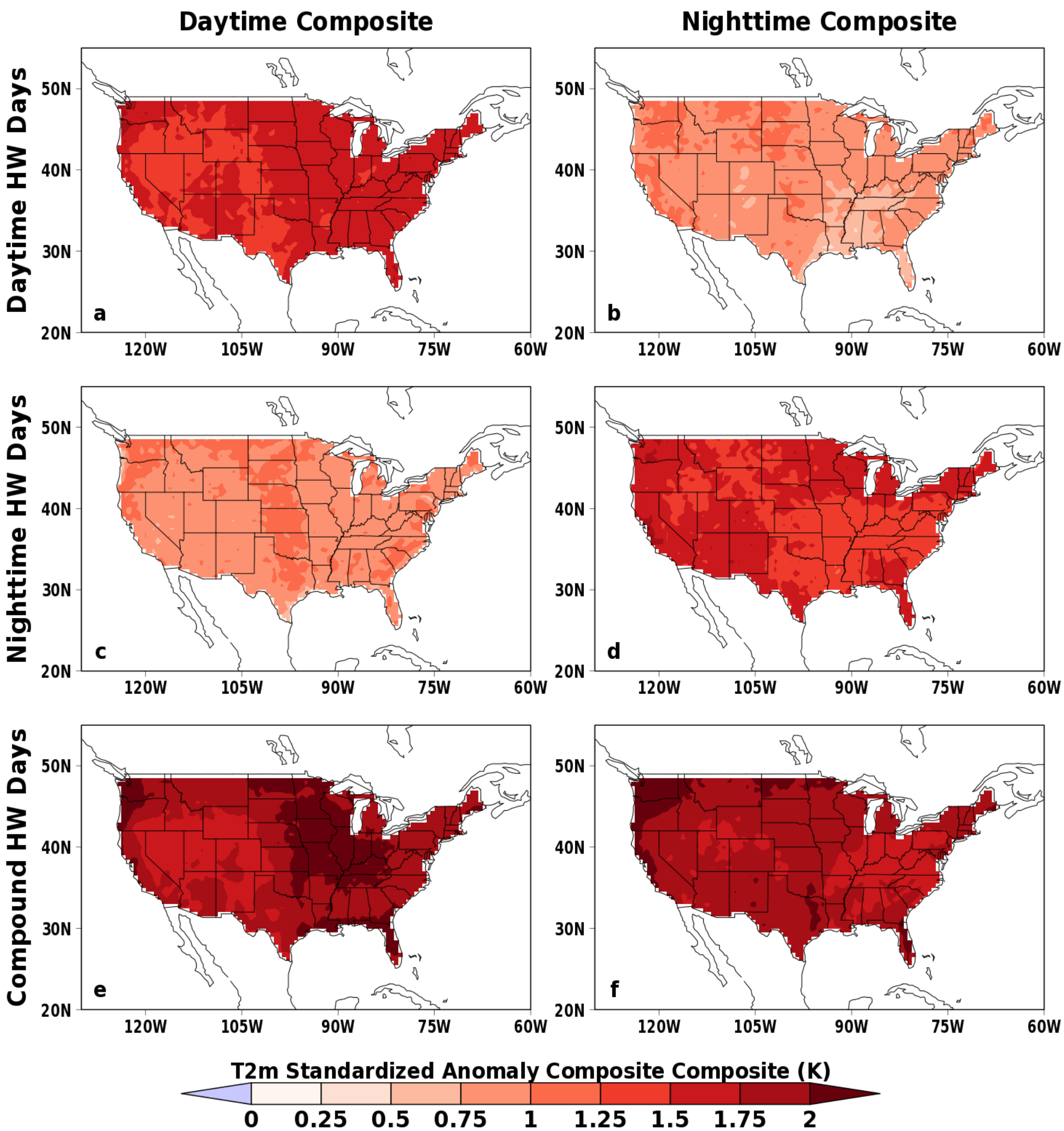

Figure 5. Composites of daily standardized anomalies in daytime 2mtemperature (°C; left column) and nighttime 2mtemperature (°C right column) for daytime heat wave days (top row), nighttime heat wave days (middle row) and compound heat wave days (bottom row).

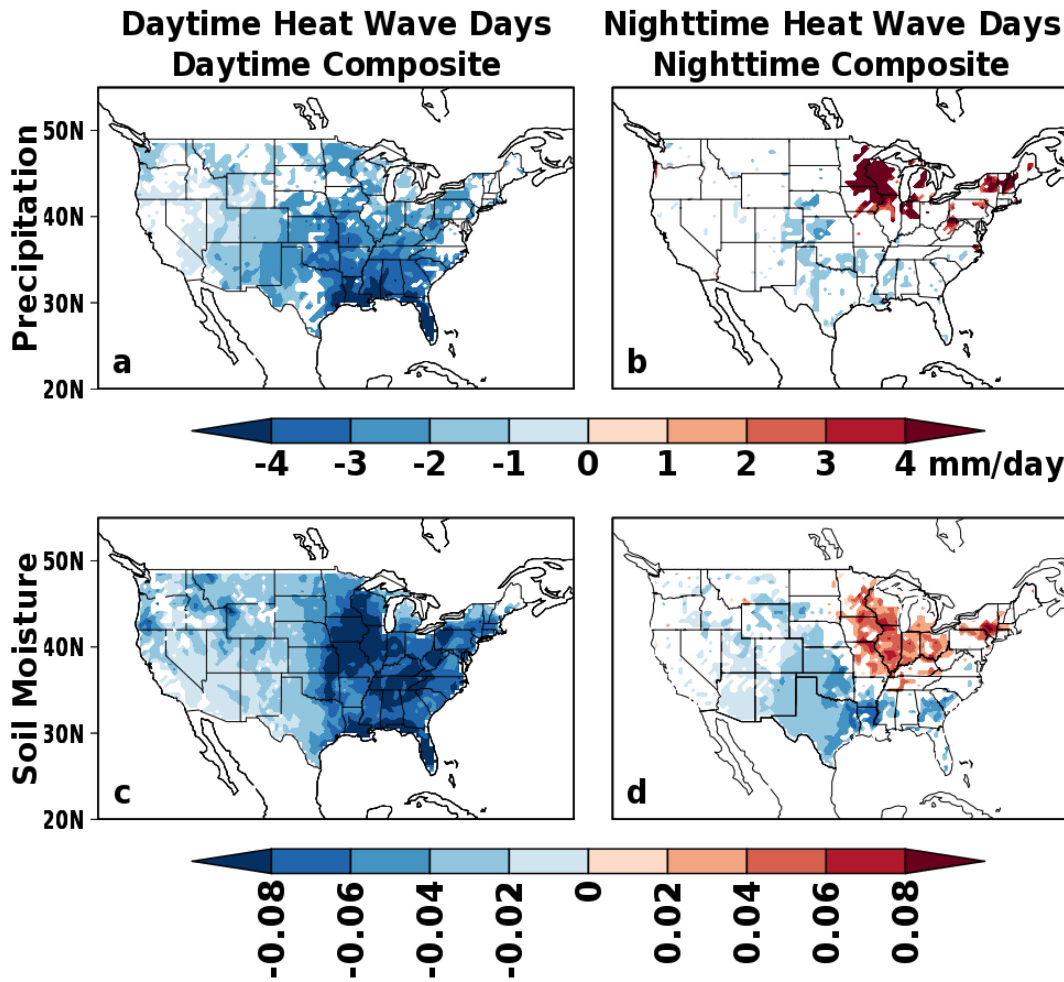

Figure 6. Composites of daily anomalies in observation corrected total precipitation (mm/day; top row) and root-zone soil moisture (dimensionless; bottom row) for daytime hours of daytime heat wave days (left column) and nighttime hours of nighttime heat wave days (right column). Regions where the composite mean is not statistically significant at the 95% confidence level are masked out.

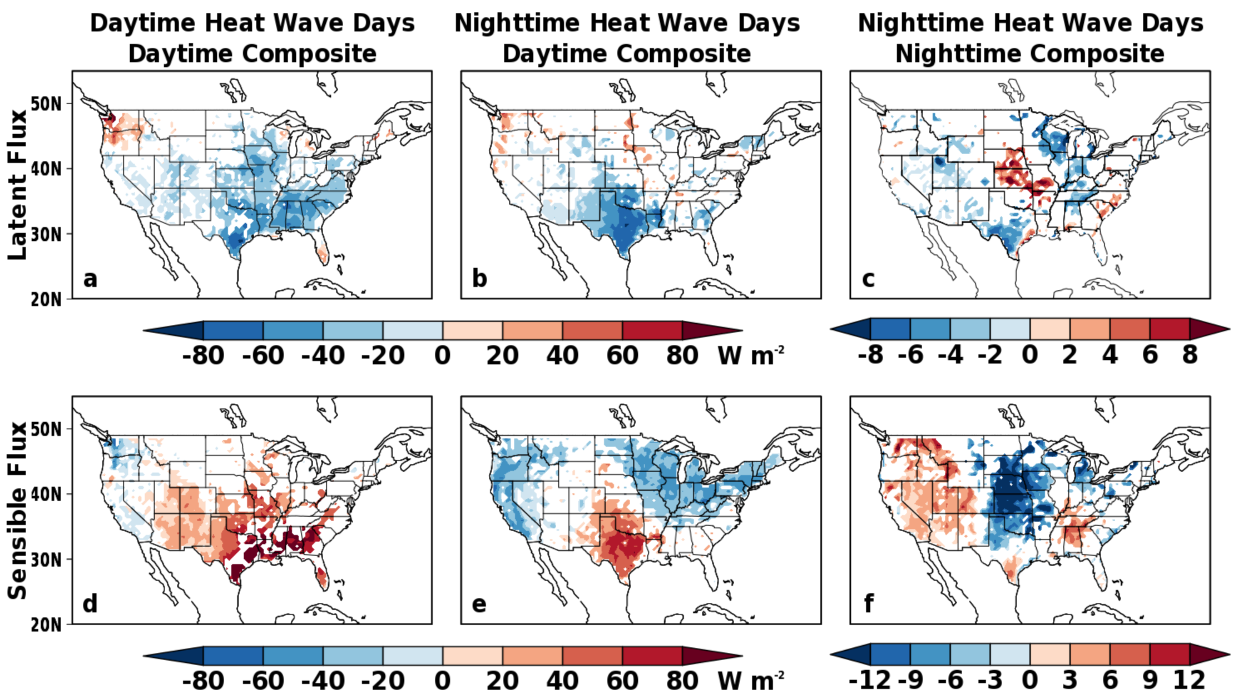

Figure 7. Composites of daily anomalies in total latent heat flux (W m^{-2}; top row) and sensible heat flux from turbulence (W m^{-2}; bottom row) for daytime hours on daytime heat wave days (left column), daytime hours on nighttime heat wave days (middle column) and nighttime hours on nighttime heat wave days (right column). Regions where the composite mean is not statistically significant at the 95% confidence level are masked out.

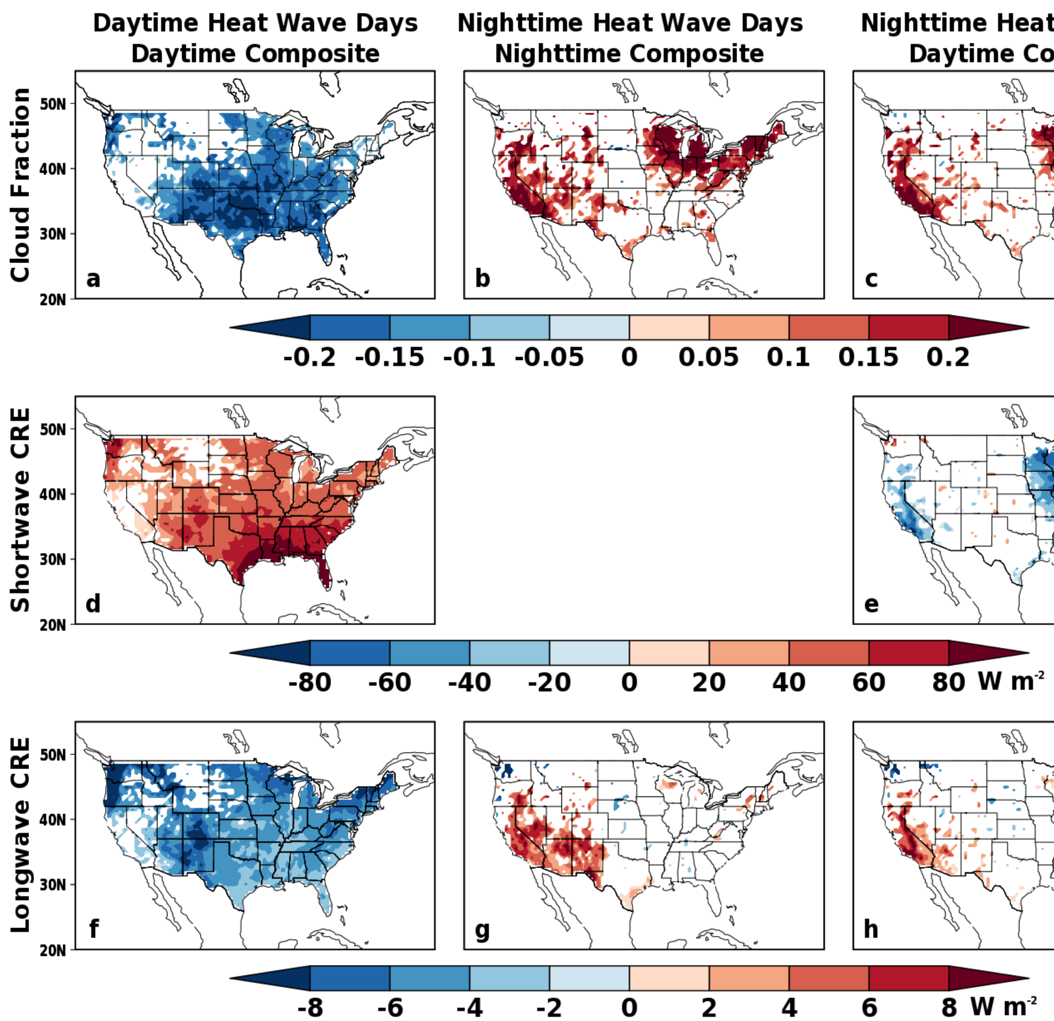

Figure 8. Composites of daily anomalies in total cloud area fraction (dimensionless; top row), shortwave CRE (W m^{-2}; middle row) and longwave CRE (W m^{-2}; bottom row) for daytime hours on daytime heat wave days (left column), nighttime hours on nighttime heat wave days (middle column) and daytime hours on nighttime heat wave days (right column). Note that there is no shortwave CRE at night. Regions where the composite mean is not statistically significant at the 95% confidence level are masked out.

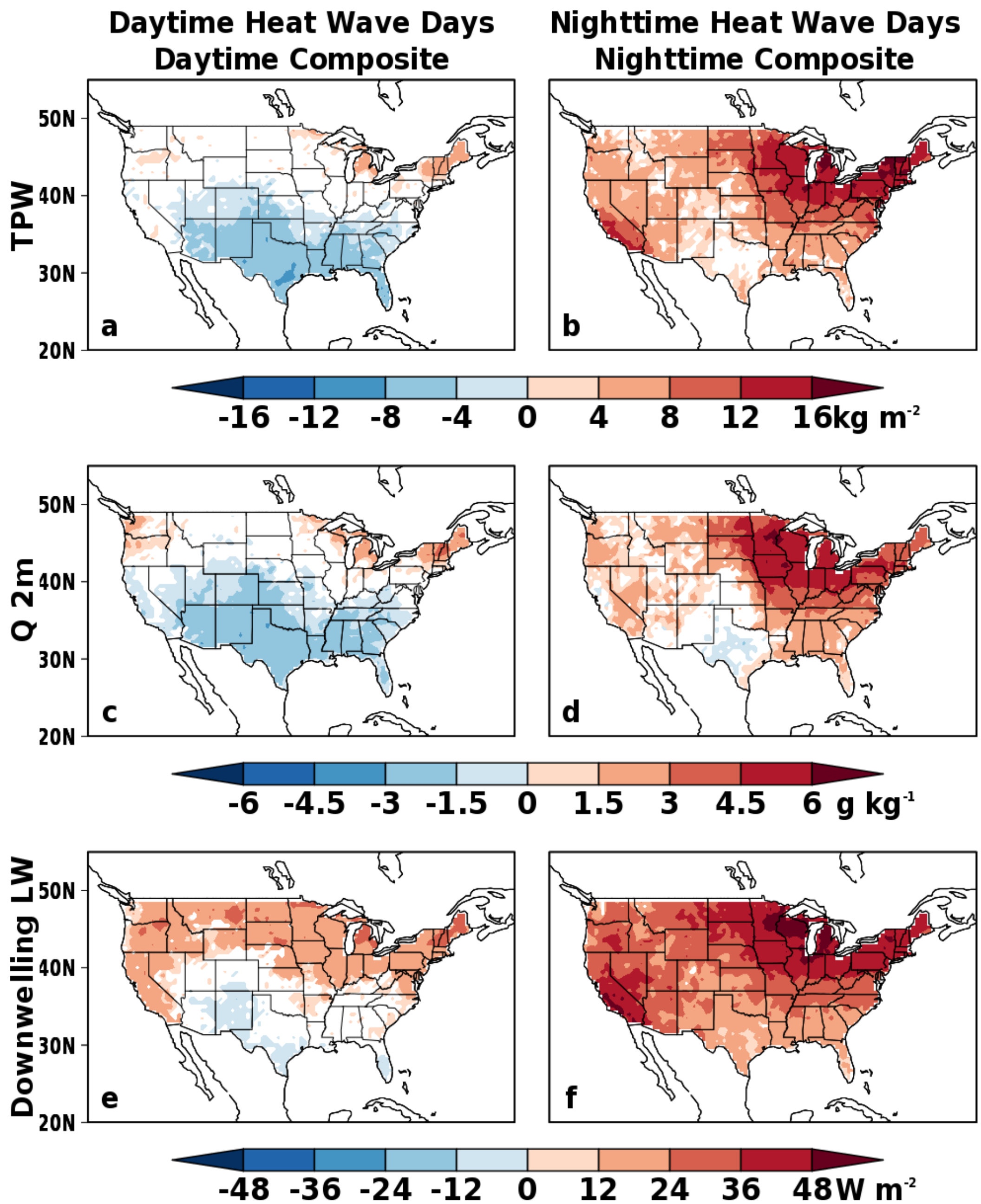

Figure 9. Composites of daily anomalies in total precipitable water vapor (kg m^{-2}; top row), 2mspecific humidity (g kg^{-1}; middle row) and surface downward longwave flux (W m^{-2}; bottom row) for daytime hours on daytime heat wave days (left column), and nighttime hours on

nighttime heat wave days (right column). Regions where the composite mean is not statistically significantly at the 95% confidence level are masked out.

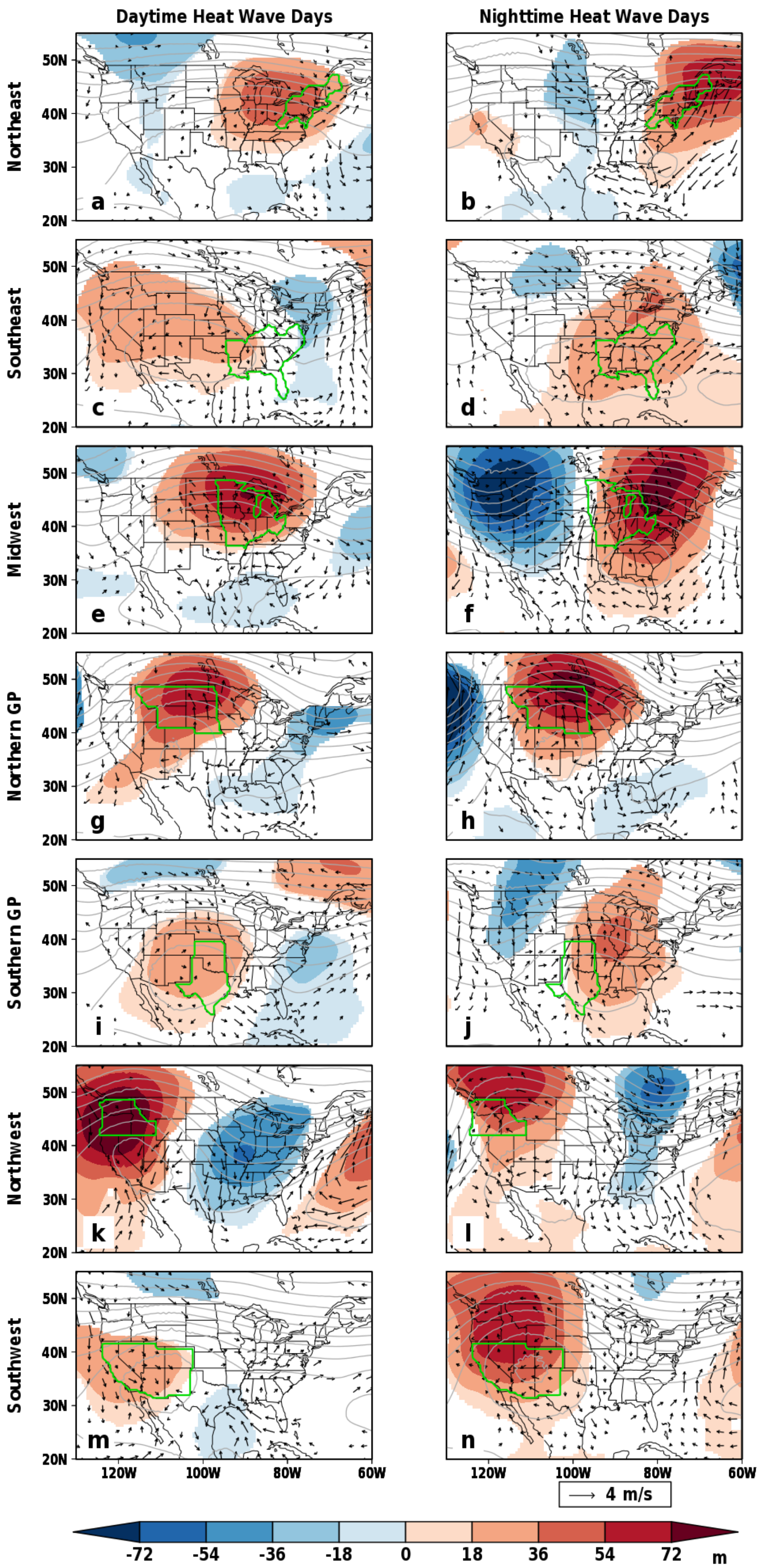

Daytime Heat Wave Days
Nighttime Heat Wave Days
Northeast
Southeast
Midwest
Northern GP
Southern GP
Northwest
Southwest
a
b
c
d
e
f
g
h
i
j
k
l
m
n
50N
40N
30N
20N
120W
100W
80W
60W
4 m/s
-72
-54
-36
-18
0
18
36
54
72
m

843

Figure 10. Composites of daily anomalies of 500-hPa heights (m; shading) and 10m winds (m/s; vectors) and daily mean 500-hPa height composites (m; grey contours) for daytime (left column) and nighttime (right column) heat wave days occurring in each NCA Region (rows). Fields are only plotted when the composite anomaly is statistically significant at the 95% confidence level. The region where area-averaged temperatures are used to find heat wave days for each region is outlined in green. See Figure 2 for the number of heat wave days incorporated into these composites for each region.

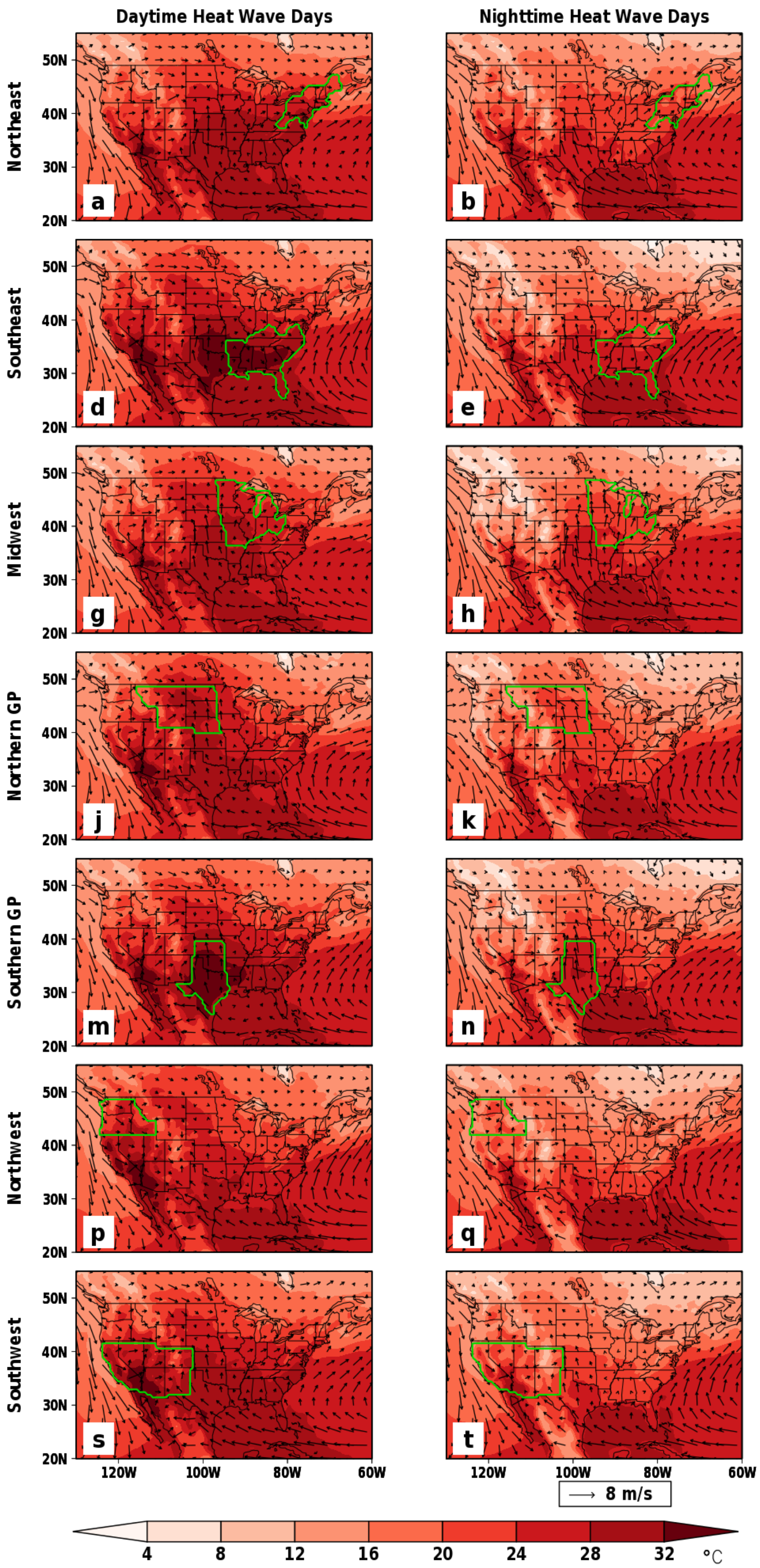
Daytime Heat Wave Days
Nighttime Heat Wave Days
Northeast
Southeast
Midwest
Northern GP
Southern GP
Northwest
Southwest
50N
40N
30N
20N
120W
100W
80W
60W
a
b
d
e
g
h
j
k
m
n
p
q
s
t
8 m/s
4
8
12
16
20
24
28
32
°C

854

Figure 11. As in Fig. 10 but for the composites of daily 2m temperature (shading; °C) and 10m winds (vectors; m/s).

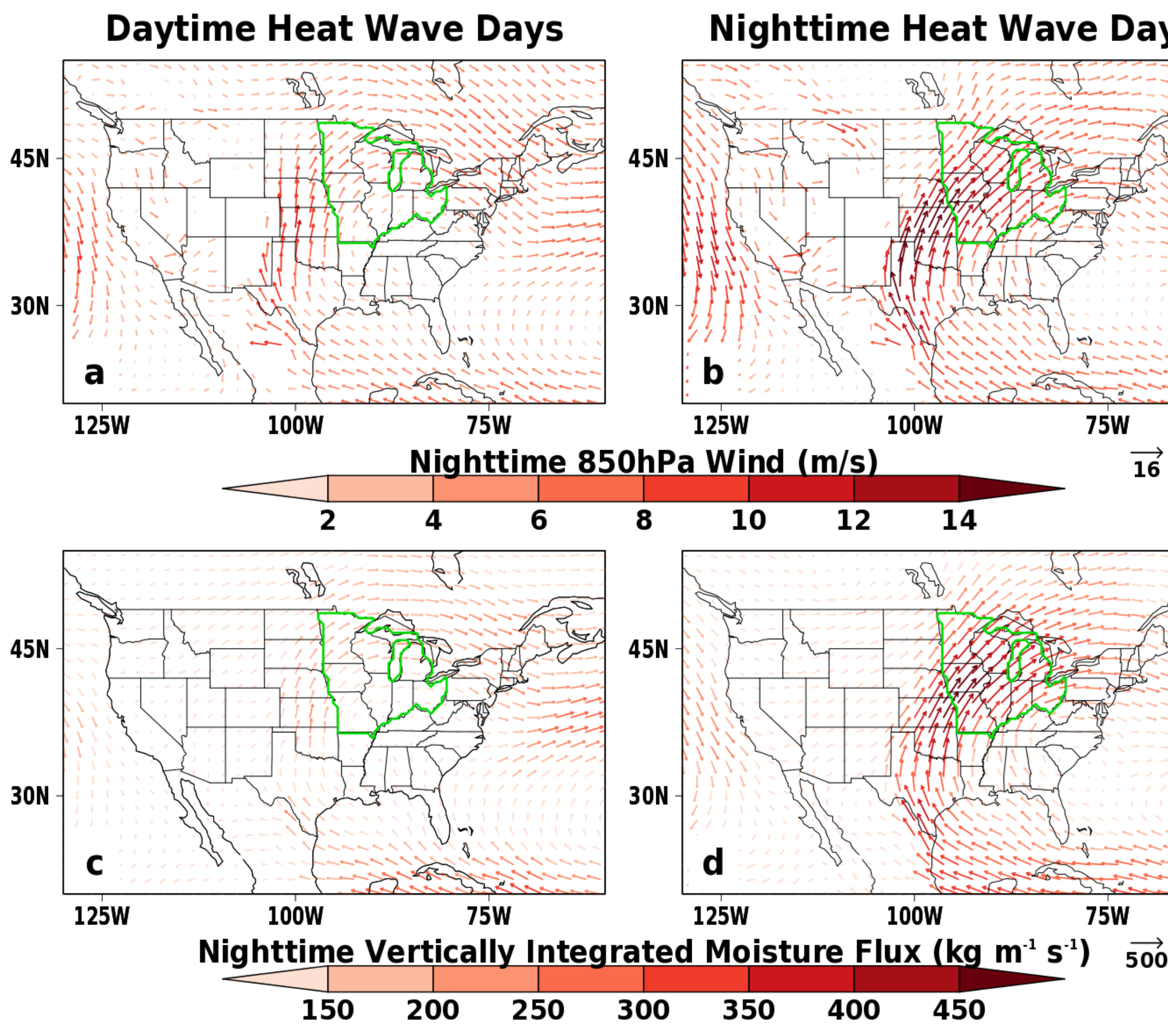

Figure 12. Composites of nighttime 850-hPa winds (m/s; top row) and nighttime vertically integrated moisture flux (kg m^{-1} s^{-1}; bottom row) for daytime (left column) and nighttime (right column) heat wave days occurring in NCA Region 3 (Midwest US, outlined in green).

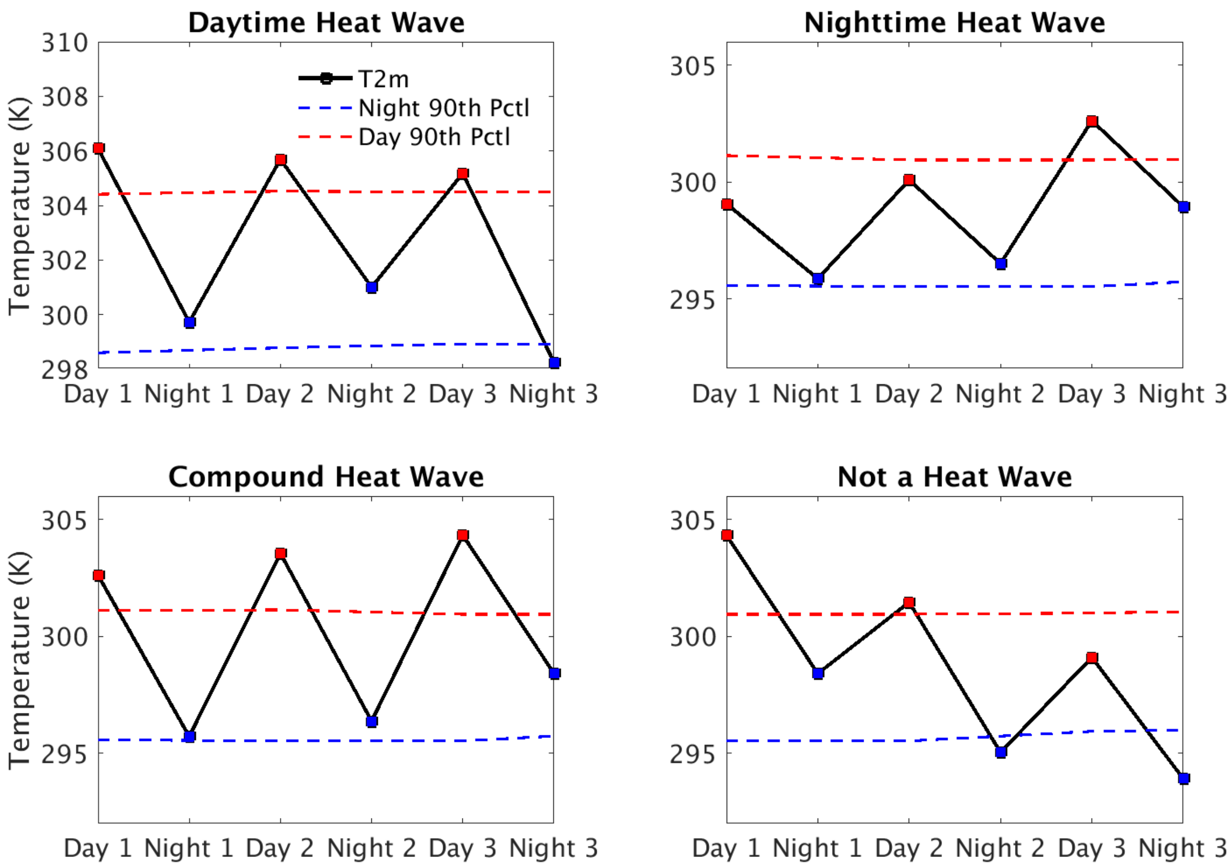

Figure A1. Schematic illustrating examples for each of the heat wave definitions. The black line shows the 2m temperature for daytime (red dots) and nighttime (blue dots) on three hypothetical days. The red (blue) line shows the calendar-day 90th percentiles for daytime (nighttime) 2m temperatures.

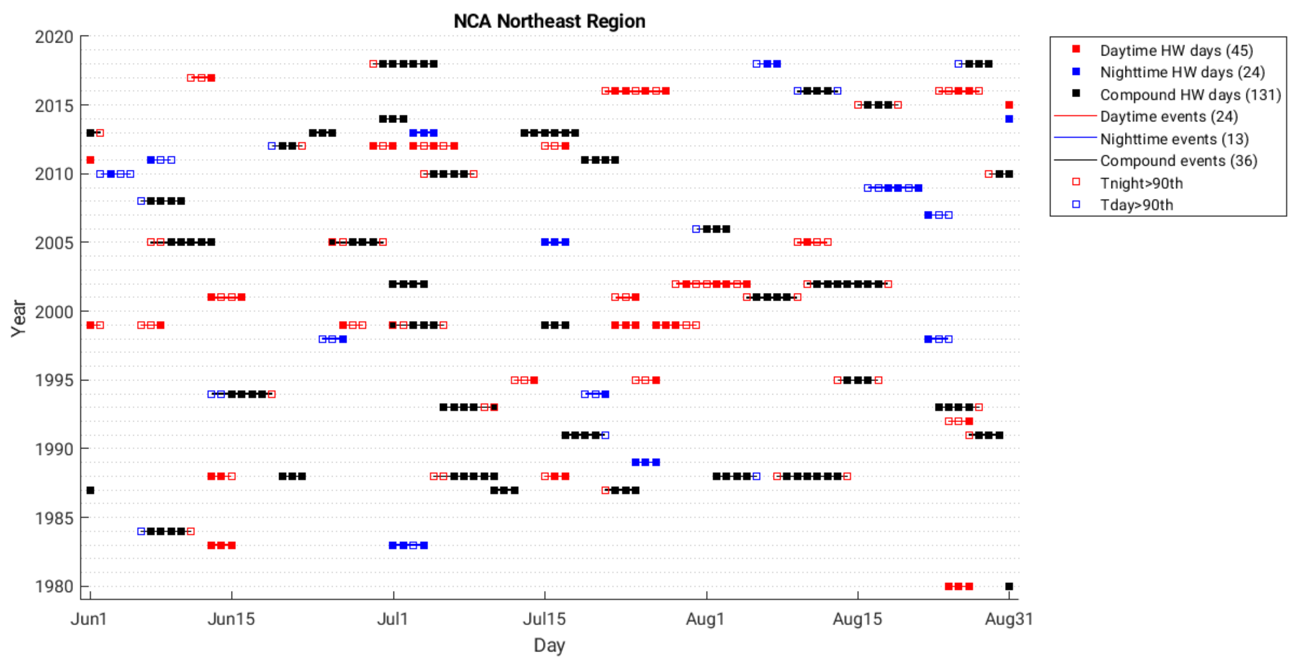

Figure A2. Heat wave days and events based on MERRA-2 2mtemperature data averaged over the Northeast NCA region. The filled in red, blue and black squares represent daytime, nighttime and compound heat wave days, respectively. The red, blue and black lines represent daytime, nighttime and compound heat wave events, respectively. Unfilled red (blue) squares represent daytime (nighttime) heat wave days where the nighttime (daytime) temperature also exceeds the 90th percentile. The numbers in parentheses in the legend indicate the number of days and events for each of the three heat wave types over JJA 1980–2018.